Conference Paper, Published Version

Yoshioka, Hidekazu; Unami, Koichi; Kawachi, Toshihiko

Partial Differential Equation Model for Spatially Distributed Statistics of Contaminant Particles in Localy One-Dimensional Open Channel Networks

PARTIAL DIFFERENTIAL EQUATION MODEL FOR SPATIALLY DISTRIBUTED STATISTICS OF CONTAMINANT PARTICLES IN LOCALLY ONE-DIMENSIONAL OPEN CHANNEL NETWORKS

Hidekazu Yoshioka[1], Koichi Unami[1], and Toshihiko Kawachi[1]

ABSTRACT

Contaminant particle dynamics in surface water flows is well described by a stochastic differential equation and its associated Kolmogorov's backward equation. This study develops a partial differential equation model (PDE model) to efficiently analyze spatially distributed statistics of contaminant particles in surface water flows. The PDE model is analytically derived from a Kolmogorov's backward equation without assuming empirical gradient type laws. Locally one-dimensional open channel networks are focused on as the domains of surface water flows. A versatile Petrov-Galerkin finite element method scheme utilizing exact solutions to local two-point boundary value problems as weight functions is developed for accurate numerical resolution of the model. Stability condition of the scheme is investigated on the basis of the *M*-matrix theory. A series of numerical test problems is carried out to verify the scheme. Numerical analysis of contaminant transport in an existing open channel network is also carried out to assess applicability of the PDE model to real life problems. Distributions of escape probability and statistical moments of residence time of contaminant particles are successfully computed with assumed dispersivity. It is concluded that our approach serves as a reliable tool for the contaminant transport analysis in open channel networks.

1. INTRODUCTION

Contaminant transport phenomena in surface water flows, such as canals, rivers, lakes, estuaries, and seas have been eagerly studied for their significant impacts on water environment and human activities. In general, such transport phenomena are analyzed using physically based mathematical models. Most of the existing models are classified as the deterministic models derived by combining mass conservation laws and empirical gradient type laws (Chatwin and Allen, 1985). However, for turbulent diffusion phenomena and dispersion phenomena, assumption of the gradient type laws is only an analogy to the well-known Fick's law for molecular diffusion phenomena. Since contaminant particle dynamics in surface water flows is inherently stochastic, more consistent approach will be necessary to take uncertainties involved in the phenomena into account properly. In

[1] Graduate Student, Graduate School of Agriculture, Kyoto University, Kitashirakawa-Oiwake-cho, Sakyo-ku, Kyoto 606-8502, Japan (yoshih@kais.kyoto-u.ac.jp)
[1]Associate Professor, Graduate School of Agriculture, Kyoto University, Kitashirakawa-Oiwake-cho, Sakyo-ku, Kyoto 606-8502, Japan (unami@adm.kais.kyoto-u.ac.jp)
[1]Emeritus Professor, Graduate School of Agriculture, Kyoto University, Kitashirakawa-Oiwake-cho, Sakyo-ku, Kyoto 606-8502, Japan (tk@adm.kais.kyoto-u.ac.jp)

order to do so, motions of contaminant particles in the flows should be understood as suitably chosen stochastic processes. Especially, stochastic differential equation (SDE) (Øksendal, 2001), the stochastic counterpart of ordinary differential equation, is known to be effective for modeling transport phenomena in surface water flows. Charles et al. (2009) analyzed two-dimensional dispersion in real shallow water based on an SDE driven by colored noise terms. Oh and Tsai (2010) modeled sediment transport in open channel flows as a jump diffusion process governed by an SDE driven by both Gaussian and Poisson white noise terms.

As well as the SDE, its associated advection diffusion equations (ADEs) the Kolmogorov's forward equation (KFE) and the Kolmogorov's backward equation (KBE) provide reasonable analytical means for contaminant transport phenomena in water bodies (Bodo et al. 1984). The KFE and the KBE respectively govern forward and backward evolution of the conditional probability density function (PDF) of particle position. Some researchers have found that application of certain mathematical operations to the KFE leads to macroscopic transport equations. Too et al. (1986) discussed longitudinal dispersion in tubular flows and analytically derived the transport equation of solute with a nonlinear reaction term. Man and Tsai (2007) derived a stochastic partial differential equation model for suspended sediments transport from a KFE. Yoshioka et al. (2012) deduced the transport equation of conservative solute based on the linearity of KFE. Their derivation technique has been extended and applied to formulate systems of transport equations of reactive substances in locally one- and horizontally two- dimensional shallow water flows (Yoshioka, 2012). On the other hand, the KBE and its related partial differential equations (PDEs) govern spatially distributed statistics of particles such as statistical moments of residence time in a domain and escape probability from a domain. Analyzing spatio-temporal evolution of the spatially distributed statistics plays a key step for well understanding and evaluating stochastic nature of contaminant transport phenomena. Naeh et al. (1990) reviewed engineering applications of the spatially distributed statistics analysis. Cai et al. (1996) developed an evaluation method for groundwater contamination process based on the analytical solutions to KBEs. A series of studies including Brannan et al. (1999, 2001) and Szurley and Duan (2001) numerically analyzed stochastic particle dynamics in geophysical vortices based on the escape probability and the mean residence time. Unami et al. (2010) utilized a KBE to assess ecological effect of hydraulic structures installed in existing drainage canals in terms of ascending probability of fish. Yoshioka et al. (2011) numerically solved KBEs to analyze stochastic contaminant particle dynamics in an existing open channel network.

This study develops a new mathematical model for the spatially distributed statistics, termed PDE model, for efficient analysis of contaminant transport phenomena in surface water flows. The model consists of a set of linear time-backward parabolic equations containing advection, diffusion, and reaction terms. Due to its Eulerian nature, the PDE model does not require cost consuming trajectory generations used in the conventional Monte-Carlo models (Lejay 2003, 2004). Locally one-dimensional open channel networks, connected graphs in which hydraulic properties such as wetted cross-sectional area and cross-section average velocity are distributed, are focused on as the domains of surface water flows. Locally one-dimensional open channel networks arise in various applied problems such as agricultural water pollution (McGechan et al. 2008), salt intrusion in estuaries (Ngyuen and Savenije, 2006), and aquatic population persistence (Grant et al., 2007).

A versatile Petrov-Galerkin finite element method (PGFEM) scheme is developed for numerical resolution of the PDE model. The scheme is categorized as the conforming finite element methods, and it has no stabilization parameters to be chosen a priori. The scheme implicitly includes internal boundary conditions in spatial discretization as in the authors' developed numerical methods (Unami 1998, Yoshioka et al. 2011) so that the channel junctions are consistently dealt with. Exact solutions to local two-point boundary value problems are utilized in determining the weight functions to generate oscillation-free numerical solutions with compact stencil. This evaluation method is referred to as the fitting technique, and it has been recognized to work well in solving the

steady ADEs (de Falco and O'Riordan, 2011), and the non-degenerate (NG-Stynes et al., 1988) and the degenerate (Valkov, 2011) unsteady ADEs in one-dimensional domains. However, to the authors' knowledge, no FEM scheme with the fitting technique has been applied to the ADEs on connected graph domains.

This paper is organized as follows. In Section 2, a concise introduction is given for locally one-dimensional open channel network as well as the SDE, the KBE, and the PDE model defined on it. In Section 3, the Petrov-Galerkin finite element formulation is presented. Stability analysis of the scheme is also conducted in this section. In Section 4, accuracy of the scheme is verified with a number of test problems in hypothetical domains. Numerical analysis of contaminant transport phenomena in an existing domain is carried out in Section 5. Section 6 provides conclusions of this study. Supplementary information is given in APPENDICES.

2. MATHEMATICAL MODEL

2.1 Definition of locally one-dimensional open channel Network

In analyzing transport phenomena in open channel systems, the one-dimensional shallow water approximation has been practically applied to flow fields (Szymkiewicz, 2010). In such a case, a locally one-dimensional open channel network extending over the horizontally two-dimensional plain defines the computational domain. A locally one-dimensional open channel network is a connected graph domain consisting of a collection of a finite number of reaches linked via a set of junctions. Hydraulic properties such as wetted cross-sectional area and cross-section average velocity are distributed on it. A finite length Jordan curve gives a reach and arbitrary position in the domain is uniquely determined by a local abscissa taken along the reach. A channel network is said to be multiply-connected if it contains at least one loop and to be simply-connected otherwise (Abbott, 1979). ADEs and SDEs defined in a locally one-dimensional open channel network generally require certain internal boundary treatments at junctions to preserve unique existence and regularity of the solutions (Von Below 1988, and Freidlin and Sheu, 2000).

2.2 SDE and associated KBE

A locally one-dimensional open channel network is taken as the domain Ω where the flow field is defined and passive contaminant particles are present. The boundary of Ω is denoted by Γ, which consists of the open boundary Γ_{O} and the wall boundary Γ_{W} with $\Gamma=\Gamma_{\mathrm{O}}\bigcup\Gamma_{\mathrm{W}}$, $\Gamma_{\mathrm{O}}\neq\varnothing$, and $\Gamma_{\mathrm{O}}\bigcap\Gamma_{\mathrm{W}}=\varnothing$. The position of a contaminant particle in Ω is modeled as a continuous stochastic process and is denoted by X_t at time t. Assuming the Markov property of X_t yields the Ito's SDE

$$\mathrm{d}X_t = V\left(t, X_t\right)\mathrm{d}t + \sqrt{2D\left(t, X_t\right)}\mathrm{d}B_t + \mathrm{d}\Phi_t \tag{1}$$

where V is the deterministic cross-sectional average velocity, $D>0$ is the dispersivity, B_t is the one-dimensional standard Brownian motion, and Φ_t is the local time (Freidlin and Sheu, 2000) that increases only at junctions. The SDE (1) describes the increment $\mathrm{d}X_t$ as a sum of the deterministic term $V\mathrm{d}t$, the stochastic term $\sqrt{2D}\mathrm{d}B_t$, and the remaining term $\mathrm{d}\Phi_t$ for the incremental law at junctions. Let $P=P\left(s,y,t,G\right)$ be the transition probability such that $X_t=x\in G$ provided that

$X_s = y$ for the past time $s < t$ for an arbitrary sub-domain G contained in Ω. The conditional PDF $p = p(s, y, t, x)$ for X_t is defined to satisfy the condition (Arnold, 1974)

$$P(s, y, t, G) = \int_G p(s, y, t, x)\,\mathrm{d}x\,. \tag{2}$$

According to Øksendal (2001), the KBE associated with the SDE (1) is given by

$$\frac{\partial p}{\partial s} + V\frac{\partial p}{\partial y} + D\frac{\partial^2 p}{\partial y^2} - Rp = \frac{\partial p}{\partial s} + L_X p = 0 \tag{3}$$

where L_X is the infinitesimal generator of X_t and $R \geq 0$ is the decay coefficient defined as

$$R = R(t, x) = \lim_{h \to +0} \frac{1}{h} P_K(t, x, h) \tag{4}$$

where $P_K(t, x, h)$ is the probability such that the particle positioned at x at the time t is killed during the time interval $(t, t+h]$. Backward evolution of p for the past time $s < t$ is uniquely determined by solving the KBE (3) with the terminal condition

$$p(t, y, t, x) = \delta(y - x) \text{ in } \Omega \tag{5}$$

and the boundary conditions

$$p(s, y, t, x) = 0 \text{ at } \Gamma_{\mathrm{O}} \tag{6}$$

and

$$D\frac{\partial p}{\partial y} = 0 \text{ at } \Gamma_{\mathrm{W}}\,. \tag{7}$$

Then, p satisfies

$$\lim_{t \to +\infty} (t - s)^k\, p(s, y, t, x) = 0 \tag{8}$$

for arbitrary non-negative integer k.

2.3 The PDE Model

The partial differential equation model (PDE model) governing escape probability from a domain and statistical moments of residence time in a domain is analytically derived from the KBE (3). This section rigorously defines these spatially distributed statistics and derives their governing equations.

2.4 Residence Time

Residence time is the total elapsed time that a particle spent in the domain before reaching the open boundary or being killed. Residence time $\tau^{s,y}$ of a particle provided that $X_s = y$ is defined as

$$\tau^{s,y} = \inf\left\{t-s \middle| t > s, X_s = y,\ X_t \in \Gamma_{\mathrm{O}} \bigcup \partial\right\} \tag{9}$$

where ∂ is the coffin state on which killed particles are put (Øksendal, 2001). By (9), the k th statistical moment of the residence time $M_k(s,y)$ is expressed using p as

$$\begin{aligned} M_k(s,y) &= \mathrm{E}^{s,y}\left[\left(\tau^{s,y}\right)^k\right] \\ &= \int_s^\infty (t-s)^k \Pr\left\{t-s < \tau^{s,y} < t-s+dt\right\} \\ &= \int_s^\infty (t-s)^k \frac{\partial}{\partial t}\Pr\left\{0 < \tau^{s,y} < t-s\right\}\mathrm{d}t \\ &= \int_s^\infty (t-s)^k \frac{\partial}{\partial t}\left[1-\int_\Omega p(s,y,t,x)\,\mathrm{d}x\right]\mathrm{d}t \\ &= -\int_s^\infty (t-s)^k \frac{\partial}{\partial t}\int_\Omega p(s,y,t,x)\,\mathrm{d}x\mathrm{d}t \end{aligned} \tag{10}$$

where $\mathrm{E}^{s,y}[\cdot]$ represents the expectation operator conditioned on s and y. Since the limit behavior of p for $t \to +\infty$ is constrained by (8), applying a partial integration to (10) results in

$$\begin{aligned} M_k(s,y) &= -\int_s^\infty (t-s)^k \frac{\partial}{\partial t}\int_\Omega p(s,y,t,x)\,\mathrm{d}x\mathrm{d}t \\ &= \left[-(t-s)^k \int_\Omega p(s,y,t,x)\,\mathrm{d}x\right]_s^\infty + \int_s^\infty \int_\Omega k(t-s)^{k-1} p(s,y,t,x)\,\mathrm{d}x\mathrm{d}t\,. \\ &= k\int_s^\infty \int_\Omega (t-s)^{k-1} p(s,y,t,x)\,\mathrm{d}x\mathrm{d}t \end{aligned} \tag{11}$$

Substituting (3) into (11) yields the governing equation of $M_k(s,y)$ as

$$\frac{\partial M_k}{\partial s} + L_X M_k = -kM_{k-1} \tag{12}$$

with the terminal condition

$$M_k(\infty, y) = 0 \ \text{ in } \ \Omega \tag{13}$$

and the boundary conditions

$$M_k(s,y) = 0 \ \text{ at } \ \Gamma_{\mathrm{O}} \tag{14}$$

and

$$D\frac{\partial M_k}{\partial y} = 0 \ \text{ at } \ \Gamma_{\mathrm{W}} \tag{15}$$

for $k \geq 1$ where $M_0(s,y)=1$ by the definition. The first order moment M_1 in particular is termed mean residence time (MRT), which is one of the most important spatially distributed statistics in application. Similar but deterministic approach based governing equation of MRT has been derived in Delhez et al. (2004) for coastal transport problems.

2.5 Escape Probability

Escape probability is the probability that a particle reaches a specified portion of the open boundary before being killed. The escape probability $E_\gamma(s,y)$ of a particle provided that $X_s = y$ reaches the portion of the open boundary $\gamma \subseteq \Gamma_O$ is expressed as

$$E_\gamma(s,y) = \Pr\left\{X_{s+\tau^{s,y}} \in \gamma \middle| X_s = y\right\}. \tag{16}$$

According to Schuss (2010), application of the Kolmogorov's representation formula to (16) yields the governing equation of $E_\gamma(s,y)$ as

$$\frac{\partial E_\gamma}{\partial s} + L_X E_\gamma = 0. \tag{17}$$

with the terminal condition

$$E_\gamma(\infty, y) = 1 \text{ in } \Omega \tag{18}$$

and the boundary conditions

$$E_\gamma(s,y) = 1 \text{ at } \gamma, \tag{19}$$

$$E_\gamma(s,y) = 0 \text{ at } \Gamma_O/\gamma, \tag{20}$$

and

$$D\frac{\partial E_\gamma}{\partial y} = 0 \text{ at } \Gamma_W. \tag{21}$$

3. FINITE ELEMENT FORMULATION

3.1 Weak Formulation

This section presents the finite element formulation for the PDE model. In order to consistently deal with singularity of junctions in the locally one-dimensional channel networks, the ADEs (12) and (17) shall be understood as the weak form

$$\int_\Omega w\frac{\partial u}{\partial s}\mathrm{d}y = -\int_\Omega wV\frac{\partial u}{\partial y}\mathrm{d}y + \int_\Omega \frac{\partial}{\partial y}(Dw)\frac{\partial u}{\partial y}\mathrm{d}y + \int_\Omega wRu\mathrm{d}y - \int_\Omega wq\mathrm{d}y \tag{22}$$

with the terminal condition

$$u(T,y) = f_T(y) \quad \text{in } \Omega \tag{23}$$

and the boundary conditions

$$u(s,y) = f_{\Gamma_O}(y) \quad \text{at } \Gamma_O \tag{24}$$

and

$$D\frac{\partial u}{\partial y} = 0 \quad \text{at } \Gamma_W \tag{25}$$

where w is arbitrary weight function in the Hilbert space $H^1(\Omega)$, T is the terminal time, $u \in H^1(\Omega)$ is the unknown, q is the source term, f_T and f_{Γ_O} are positive functions. The left hand side of (22) vanishes in steady problems. Based on the above weak formulation, internal boundary conditions at junctions are implicitly taken into account as shown in the next section.

3.2 Spatial Discretization

Spatial discretization of the weak form (22) is performed within the fitting Petrov-Galerkin framework. The domain Ω is firstly divided into a computational mesh consisting of elements bounded by two nodes, so that any junction exactly falls on one of the nodes. The elements and the nodes are respectively indexed with the natural numbers. The total numbers of elements and nodes are respectively denoted by N_e and N_n. The i th node is denoted by P_i. The k th element is denoted by Ω_k. The length of Ω_k is represented by l_k. The number of elements connected to P_i is denoted by $\nu(i)$. The j th element connected to P_i is referred to as the $\kappa(i,j)$ th element $\Omega_{\kappa(i,j)}$. There are two nodes that bound $\Omega_{\kappa(i,j)}$; one of them is the i th node P_i, and the other is referred to as the $\mu(i,j)$ th node $P_{\mu(i,j)}$. A schematic sketch of the computational mesh is shown in Figure 1.

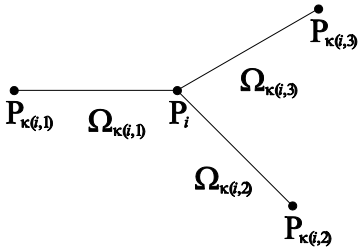

Figure 1 A schematic sketch of the computational mesh around the node P_i ($\nu(i) = 3$).

The direction of the y abscissa in $\Omega_{\kappa(i,j)}$ is identified with the sign parameter $\sigma_{i,j}$, which is equal to 1 when y is directed to $P_{\mu(i,j)}$ and is equal to -1 otherwise. The known functions V and R are

attributed to the elements as constant values, while D and q are attributed to the elements as linear functions which may be discontinuous at the nodes. According to Benichou and Debsbois (2009), such discontinuities of the known functions do not affect well-posedness of the problem. The discretized V and R in Ω_k are denoted as V_k and R_k, respectively. The discretized D and q in $\Omega_{\kappa(i,j)}$ are respectively denoted as $D_{i,j}$ and $q_{i,j}$, and these are given by

$$\phi_{i,j} = \begin{cases} \phi_{i,j,0} + \left(\phi_{i,j,1} - \phi_{i,j,0}\right) z_{i,j}, \ y \in \Omega_{\kappa(i,j)} \\ 0, \ \text{Otherwise} \end{cases} \tag{26}$$

with the local abscissa

$$z_{i,j} = \frac{y - y_i}{\sigma_{i,j} l_{\kappa(i,j)}} \ \text{ in } \ \Omega_{\kappa(i,j)} \tag{27}$$

where $\phi_{i,j,0}$ and $\phi_{i,j,1}$ are the left hand side limit in $\Omega_{\kappa(i,j)}$

$$\phi_{i,j,0} = \lim_{y \to y_i \text{ in } \Omega_{\kappa(i,j)}} \phi \tag{28}$$

and the right hand limit in $\Omega_{\kappa(i,j)}$

$$\phi_{i,j,1} = \lim_{y \to y_{\mu(i,j)} \text{ in } \Omega_{\kappa(i,j)}} \phi, \tag{29}$$

y_i and $y_{\mu(i,j)}$ represent y at P_i and at $\mathrm{P}_{\mu(i,j)}$, and ϕ corresponds to D or q. The unknown u in $\Omega_{\kappa(i,j)}$ is linearly interpolated as

$$u = u_i + \left(u_{\mu(i,j)} - u_i\right) z_{i,j} \tag{30}$$

to ensure $u \in H^1(\Omega)$. On the basis of the fitting technique, exact solutions to local two-point boundary value problems are utilized to determine the weight function w in order to generate oscillation free numerical solutions. The weight function associated with the node P_i is denoted as w_i, and is determined to solve the two-point boundary value problems

$$D_{i,j,0} \frac{\partial^2 w_i}{\partial y^2} - V_{\kappa(i,j)} \frac{\partial w_i}{\partial y} - R_{\kappa(i,j)} w_i = 0 \ \text{ in } \ \Omega_{\kappa(i,j)} \tag{31}$$

$$w_i(x_i) = 1, \ \ w_i\left(x_{\mu(i,j)}\right) = 0 \tag{32}$$

for $1 \le j \le \nu(i)$. Since the support ω_i of w_i is given by closure of the additive set of elements

$$\omega_i = \overline{\bigcup_{j=1}^{\nu(i)} \Omega_{\kappa(i,j)}}, \tag{33}$$

spatial discretization in the PGFEM scheme is carried out with compact stencil. Exact solutions to (31) and (32) are calculated as

$$w_i = \frac{\exp\left(\lambda_{i,j}^{+} + \lambda_{i,j}^{-} z_{i,j}\right) - \exp\left(\lambda_{i,j}^{-} + \lambda_{i,j}^{+} z_{i,j}\right)}{\exp\left(\lambda_{i,j}^{+}\right) - \exp\left(\lambda_{i,j}^{-}\right)} \quad \text{in } \Omega_{\kappa(i,j)} \tag{34}$$

where $\lambda_{i,j}^{\pm}$ are the non-dimensional parameters given by

$$\lambda_{i,j}^{\pm} = \frac{1}{2}\left(\frac{\sigma_{i,j} V_{\kappa(i,j)} l_{\kappa(i,j)}}{D_{i,j,0}} \pm \sqrt{\left(\frac{V_{\kappa(i,j)} l_{\kappa(i,j)}}{D_{i,j,0}} \right)^2 + \frac{4 R_{\kappa(i,j)} l_{\kappa(i,j)}^2}{D_{i,j,0}}} \right). \tag{35}$$

However, the l'Hospital's rule is applied to (34) for degenerate cases as

$$w_i = \frac{\exp\left(P_{i,j}\right) - \exp\left(P_{i,j} z_{i,j}\right)}{\exp\left(P_{i,j}\right) - 1} \quad \text{in } \Omega_{\kappa(i,j)} \tag{36}$$

with

$$P_{i,j} = \frac{\sigma_{i,j} V_{\kappa(i,j)} l_{\kappa(i,j)}}{D_{i,j,0}} \tag{37}$$

when $V_{\kappa(i,j)} \neq 0$ and $R_{\kappa(i,j)} = 0$, and

$$w_i = 1 - z_{i,j} \quad \text{in } \Omega_{\kappa(i,j)} \tag{38}$$

when $V_{\kappa(i,j)} = 0$ and $R_{\kappa(i,j)} = 0$. Since $R_{\kappa(i,j)}$ is greater than or equal to 0, w_i in the sub-domain $\Omega_{\kappa(i,j)}$ monotonically decreases from 1 at y_i to 0 at $y_{\mu(i,j)}$ (Gilberg and Trundinger, 1977). Therefore, considering the direction of the y abscissa in $\Omega_{\kappa(i,j)}$ yields the inequality

$$\sigma_{i,j} \frac{\partial w_i}{\partial y} < 0 \quad \text{in } \Omega_{\kappa(i,j)}. \tag{39}$$

Substituting $w = w_i$ into (22) yields

$$\int_{\omega_i} w_i \frac{\partial u}{\partial s} \mathrm{d}y = -\int_{\omega_i} w_i V \frac{\partial u}{\partial y} \mathrm{d}y + \int_{\omega_i} \frac{\partial}{\partial y}\left(D w_i\right) \frac{\partial u}{\partial y} \mathrm{d}y + \int_{\omega_i} w_i R u \mathrm{d}y - \int_{\omega_i} w_i q \mathrm{d}y \,. \tag{40}$$

The left hand side of (40) is calculated as

$$\begin{aligned}\int_{\omega_i} w_i \frac{\partial u}{\partial s}\mathrm{d}y &= \sum_{j=1}^{\nu(i)} \int_{\Omega_{\kappa(i,j)}} w_i \frac{\partial u}{\partial s}\mathrm{d}y \\ &= \sum_{j=1}^{\nu(i)} \left(\int_{\Omega_{\kappa(i,j)}} w_i \frac{\partial}{\partial s}\left(u_i + \frac{u_{\mu(i,j)} - u_i}{\sigma_{i,j} l_{\kappa(i,j)}}\left(y - y_i\right)\right)\mathrm{d}y \right). \\ &= \sum_{j=1}^{\nu(i)} \left(I_{i,j,0}\frac{\mathrm{d}u_i}{\mathrm{d}s} + I_{i,j,1}\frac{\mathrm{d}u_{\mu(i,j)}}{\mathrm{d}s} \right)\end{aligned} \tag{41}$$

where the integrals $I_{i,j,0}$ and $I_{i,j,1}$ are given by

$$I_{i,j,0} = \int_{\Omega_{\kappa(i,j)}} w_i \left(1 - \frac{y - y_i}{\sigma_{i,j} l_{\kappa(i,j)}}\right)\mathrm{d}y, \quad I_{i,j,1} = \int_{\Omega_{\kappa(i,j)}} w_i \left(\frac{y - y_i}{\sigma_{i,j} l_{\kappa(i,j)}}\right)\mathrm{d}y\,. \tag{42}$$

Exact expressions of $I_{i,j,0}$ and $I_{i,j,1}$ are presented in APPENDIX A. The last term of the right hand side of (40) is calculated as

$$\begin{aligned}-\int_{\omega_i} w_i q \mathrm{d}x &= -\sum_{j=1}^{\nu(i)} \int_{\Omega_{\kappa(i,j)}} w_i q_{\kappa(i,j)}\mathrm{d}x \\ &= -\sum_{j=1}^{\nu(i)} \left(I_{i,j,0} q_{i,j,0} + I_{i,j,1} q_{i,j,1} \right)\end{aligned}\,. \tag{43}$$

Since u is element-wise linear, the second term of the right hand side of (40) is calculated as

$$\begin{aligned}\int_{\omega_i} \frac{\partial}{\partial y}\left(Dw_i\right)\frac{\partial u}{\partial y}\mathrm{d}y &= \sum_{j=1}^{\nu(i)} \int_{\Omega_{\kappa(i,j)}} \frac{\partial}{\partial y}\left(Dw_i\right)\frac{\partial u}{\partial y}\mathrm{d}y \\ &= \sum_{j=1}^{\nu(i)} \left.\frac{\partial u}{\partial y}\right|_{\Omega_{\kappa(i,j)}} \int_{\Omega_{\kappa(i,j)}} \frac{\partial}{\partial y}\left(Dw_i\right)\mathrm{d}y \\ &= \sum_{j=1}^{\nu(i)} \left.\frac{\partial u}{\partial y}\right|_{\Omega_{\kappa(i,j)}} \left(-\sigma_{i,j} D_{i,j,0}\right) \\ &= \sum_{j=1}^{\nu(i)} \left.\frac{\partial u}{\partial y}\right|_{\Omega_{\kappa(i,j)}} \int_{\Omega_{\kappa(i,j)}} D_{i,j,0}\frac{\partial w_i}{\partial y}\mathrm{d}y \\ &= \sum_{j=1}^{\nu(i)} \int_{\Omega_{\kappa(i,j)}} D_{i,j,0}\frac{\partial w_i}{\partial y}\frac{\partial u}{\partial y}\mathrm{d}y\end{aligned}\,. \tag{44}$$

By (44), the first, the second, and the third terms of the right hand side of (40) are recast as

$$
\begin{aligned}
&-\int_{\omega_i} w_i V \frac{\partial u}{\partial y}\mathrm{d}y + \int_{\omega_i} \frac{\partial}{\partial y}\left(D w_i\right)\frac{\partial u}{\partial y}\mathrm{d}y + \int_{\omega_i} w_i R u \mathrm{d}y \\
&= \sum_{j=1}^{\nu(i)}\left(-\int_{\Omega_{\kappa(i,j)}} w_i V_{\kappa(i,j)} \frac{\partial u}{\partial y}\mathrm{d}y + \int_{\Omega_{\kappa(i,j)}} \frac{\partial}{\partial y}\left(D w_i\right)\frac{\partial u}{\partial y}\mathrm{d}y + \int_{\Omega_{\kappa(i,j)}} w_i R_{\kappa(i,j)} u \mathrm{d}y \right) \\
&= \sum_{j=1}^{\nu(i)}\left(-\int_{\Omega_{\kappa(i,j)}} \left(V_{\kappa(i,j)} w_i - D_{i,j,0}\frac{\partial w_i}{\partial y}\right)\frac{\partial u}{\partial y}\mathrm{d}y + \int_{\Omega_{\kappa(i,j)}} w_i R_{\kappa(i,j)} u \mathrm{d}y \right) \\
&= -\sum_{j=1}^{\nu(i)}\left(\left[\left(w_i V_{\kappa(i,j)} - D_{i,j,0}\frac{\partial w_i}{\partial y}\right) u \right]_{\partial\Omega_{\kappa(i,j)}} + \int_{\Omega_{\kappa(i,j)}} \left(D_{i,j,0}\frac{\partial^2 w_i}{\partial y^2} - V_{\kappa(i,j)}\frac{\partial w_i}{\partial y} - R_{\kappa(i,j)} w_i \right) u \mathrm{d}y \right)
\end{aligned}
\tag{45}
$$

Since w_i is the solution to (31) and (32), the second term of the right hand side of (45) vanishes. Finally, (40) results in the ordinary differential equation (ODE)

$$
\sum_{j=1}^{\nu(i)}\left(I_{i,j,0}\frac{\mathrm{d}u_i}{\mathrm{d}s} + I_{i,j,1}\frac{\mathrm{d}u_{\mu(i,j)}}{\mathrm{d}s}\right) = -\sum_{j=1}^{\nu(i)}\left[u\left(w_i V_{\kappa(i,j)} - D_{i,j,0}\frac{\partial w_i}{\partial y}\right)\right]_{\partial\Omega_{\kappa(i,j)}} - \sum_{j=1}^{\nu(i)}\left(I_{i,j,0} q_i + I_{i,j,1} q_{\mu(i,j)}\right). \tag{46}
$$

When the node $\mathrm{P_i}$ falls on a junction, the ODE (46) serves as an internal boundary condition and thus the present PGFEM scheme consistently deals with junctions without any special treatment.

3.3 Temporal Discretization

Assembling (46) for all i yields the system of ODEs

$$
-\mathrm{M}\frac{\mathrm{d}\mathbf{u}}{\mathrm{d}s} = \mathrm{N}\mathbf{u} + \mathbf{b} \tag{47}
$$

where $\mathbf{u} = \left[u_i\right]$ is the N_n-dimensional nodal solution vector, $\mathrm{M} = \left[\mathrm{M}_{i,k}\right]$ and $\mathrm{N} = \left[\mathrm{N}_{i,k}\right]$ are the $N_\mathrm{n} \times N_\mathrm{n}$-dimensional matrices, and $\mathbf{b} = \left[b_i\right]$ is the N_n-dimensional vector independent of $\mathbf{u}$. The system of ODEs (47) is integrated backward in time by the θ-method (Knabner and Angermann, 2003) starting from the terminal condition (23) with imposing the boundary conditions (24) and (25) . Applying the θ-method to (47) obtains the recursion

$$
\begin{aligned}
-\left(\theta\mathrm{M}^{(m+1)} + \left(1-\theta\right)\mathrm{M}^{(m)}\right)\frac{\mathbf{u}^{(m+1)} - \mathbf{u}^{(m)}}{\Delta s} &= -\overline{\mathrm{M}}^{(m)}\frac{\mathbf{u}^{(m+1)} - \mathbf{u}^{(m)}}{\Delta s} \\
&= \left(\theta\mathrm{N}^{(m+1)} + \left(1-\theta\right)\mathrm{N}^{(m)}\right)\left(\theta\mathbf{u}^{(m+1)} + \left(1-\theta\right)\mathbf{u}^{(m)}\right) \\
&\quad + \theta\mathbf{b}^{(m+1)} + \left(1-\theta\right)\mathbf{b}^{(m)} \\
&= \overline{\mathrm{N}}^{(m)}\left(\theta\mathbf{u}^{(m+1)} + \left(1-\theta\right)\mathbf{u}^{(m)}\right) + \theta\mathbf{b}^{(m+1)} + \left(1-\theta\right)\mathbf{b}^{(m)}
\end{aligned}
\tag{48}
$$

where $\Delta s < 0$ is the fixed time increment, the superscript $\left(m\right)$ represents the value at the time $s = T + m\Delta s$, and $\overline{\mathrm{M}}^{(m)}$ and $\overline{\mathrm{N}}^{(m)}$ are the $N_\mathrm{n} \times N_\mathrm{n}$-dimensional matrices given by

$$\overline{\mathrm{M}}^{(m)} = \theta \mathrm{M}^{(m+1)} + \left(1-\theta\right)\mathrm{M}^{(m)} \tag{49}$$

and

$$\overline{\mathrm{N}}^{(m)} = \theta \mathrm{N}^{(m+1)} + \left(1-\theta\right)\mathrm{N}^{(m)}. \tag{50}$$

Straightforward calculations show that $\mathrm{M}^{(m)}$ is positive definite and $-\mathrm{N}^{(m)}$ is an *M*-matrix (APPENDIX B).

3.4 Stability Analysis

Stability of the PGFEM scheme is analyzed on the basis of the *M*-matrix theory (Hundsdorfer and Verwer, 2007). Here, a numerical scheme is said to be stable if it generates oscillation-free numerical solutions. The vector $\mathbf{b}$ is set as the null vector throughout the stability analysis since it makes no contribution to stability of the scheme.

3.5 Stability for steady Problems

In steady problems, the system of ODEs (47) reduces to the linear algebraic equation

$$-\mathrm{N}\mathbf{u} = \mathbf{0} \tag{51}$$

where $\mathbf{0}$ is the N_{n} -dimensional null vector. Since inverse of an *M*-matrix is positive definite, inverse of $-\mathrm{N}$ is positive definite as well, showing that the scheme satisfies the elliptic discrete maximum principle (Idelsohn et al, 1996) and is unconditionally stable for steady problems.

3.6 Stability for unsteady Problems

It has been well recognized that FEM schemes produce unphysical oscillatory solutions for unsteady ADEs due to the positive-definiteness of mass-matrix, even if the time increment is taken sufficiently fine. A simple and efficient way to cope with this issue is to lump the mass-matrix (Quarteroni and Valli, 2008). In this study, the matrix $\mathrm{M}^{(m)}$ is lumped as

$$\mathrm{M}_{i,k}^{(m)} \to \mathrm{M}_{i,k}^{(m)} = \begin{cases} \sum_{j=1}^{\nu(i)} \left(I_{i,j,0} + I_{i,j,1} \right), & i = k \\ 0, \quad \text{Otherwise} \end{cases}. \tag{52}$$

Then, the system of ODEs (47) results in

$$-\mathrm{M}\frac{\mathrm{d}\mathbf{u}}{\mathrm{d}s} = \mathrm{N}\mathbf{u}, \tag{53}$$

leading to the recursion

$$-\left(\frac{1}{\Delta s}\overline{\mathrm{M}}^{(m)}+\theta\overline{\mathrm{N}}^{(m+1)}\right)\mathbf{u}^{(m+1)}=\left(-\frac{1}{\Delta s}\overline{\mathrm{M}}^{(m)}+(1-\theta)\overline{\mathrm{N}}^{(m)}\right)\mathbf{u}^{(m)} \tag{54}$$

where

$$\overline{\mathrm{M}}^{(m)}=\theta\mathrm{M}^{(m+1)}+(1-\theta)\mathrm{M}^{(m)}. \tag{55}$$

According to Mincsovics (2010), the PGFEM scheme is stable with satisfying the parabolic discrete maximum principle if $-\Delta s$ is chosen sufficiently small so that

$$0<-\Delta s<\min_{i,m}\left\{-\frac{\overline{\mathrm{M}}_{i,i}^{(m)}}{(1-\theta)\overline{\mathrm{N}}_{i,i}^{(m)}}\right\} \tag{56}$$

holds. This inequality is automatically satisfied in the case of $\theta=1$.

4. NUMERICAL TESTS

The PGFEM scheme is verified with a number of test problems in a one-dimensional interval and in a simply-connected open channel network. Computed solutions are compared with analytical or reference solutions. The time increment Δs is chosen so that the inequality (56) is fulfilled.

4.1 Test Problems in a one-dimensional Interval

The PGFEM scheme is firstly applied to one-dimensional test problems to examine its accuracy. The unit interval $(0,1)$ is taken as the computational domain Ω, which is divided into $N_{\mathrm{e}}=100$ uniform elements with $N_{\mathrm{n}}=101$ nodes. Here, two test problems Tests 1D-a and 1D-b are examined. The known functions V, D, R, q, the terminal condition (T.C.), and the boundary conditions (B.C.) are specified in Tests 1D-a and 1D-b as summarized in Table 1 where d and r are positive constants, and H is the Heaviside step function. Test 1D-a is a steady problem with a flow turning point at $x=0.5$ and Test 1D-b is an unsteady problem with continuously varying diffusivity. Solution of Test 1D-a exhibits a sudden transition around the flow turning point $x=0.5$ when both D and R are small (Farrel et al., 2004), which is difficult to compute with the conventional numerical schemes. Numerical resolution of Test 1D-b requires both spatial and temporal accuracy. In Test 1D-b, the terminal time T, the time increment Δs, and the parameter θ are set as 0.5, -0.01, and 0.5, respectively. Since the analytical solution of Test 1D-b is not known, numerical solution on $N_{\mathrm{e}}=1{,}000$ uniform elements with the time increment $\Delta s=-0.001$ is regarded as the reference solution. Comparisons of the computed and the analytical solutions of Test 1D-a for $(d,r)=(0.0001,1)$ and $(d,r)=(0.0001,10{,}000)$ are shown in Figure 2, and comparisons of the computed and the reference solutions of Test 1D-b for $(d,r)=(0.01,1)$ and $(d,r)=(0.0001,1)$ are shown in Figure 3 and Figure 4. Figure 2 shows that the PGFEM scheme exhibits excellent accuracy for the steady problems, while Figure 3 and Figure 4 show that the scheme produces overly smoothed solutions for the unsteady problems with small diffusivity. This is due to the mass lumping technique employed in the scheme. As reported in Guo and Stynes (1994a, 1994b), lumped

FEM schemes generally have excessive apparent numerical diffusivity. The PGFEM scheme developed in this study is not an exception. However, non-lumped FEM schemes generally cannot satisfy the parabolic discrete maximum principle which ensures temporal stability. Thus, there is a tradeoff between temporal accuracy and stability of the FEM schemes, and which should be chosen depends on the purpose of analysis. Since this study focuses on analyzing non-negative spatially distributed statistics, negative numerical solutions should not be present. Therefore, the mass lumping employed in this study is a reasonable option to obtain physically meaningful solutions.

Table 1 Computational conditions specified for Tests 1D-a and 1D-b.

Test	V	D	R	q	T.C.	B.C.
1D-a	$1.5H(x-0.5)-1$	0.0001	r	1	Not specified	$u(t,0)=u(t,1)=0$
1D-b	1	$d(1+y)$	1	0	$u(T,y)=1$	$u(t,0)=u(t,1)=0$

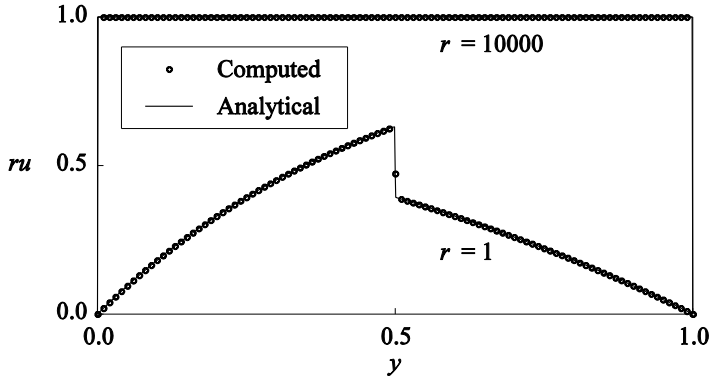

Figure 2 Comparisons of computed and analytical solutions for Test 1D-a with $r=1$ and $r=10,000$.

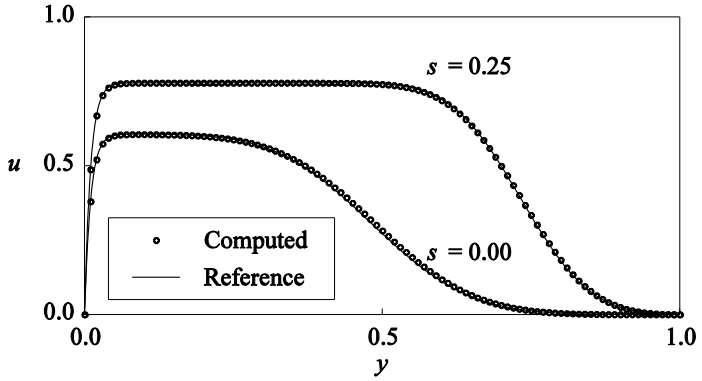

Figure 3 Comparisons of computed and reference solutions for Test 1D-a with $d=0.01$.

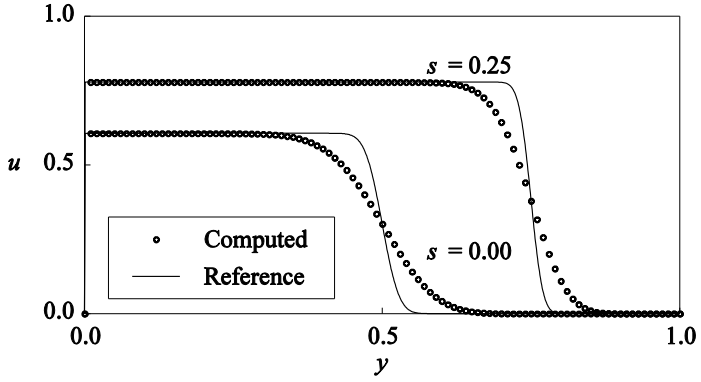

Figure 4 Comparisons of computed and reference solutions for Test 1D-a with $d = 0.0001$.

4.2 Test Problems in a simply-connected open channel Network

The PGFEM scheme is examined to compute MRT distributions based on the ADE (12), for the purpose of verifying its ability to deal with junctions. The hypothetical simply-connected open channel network in Ramirez (2011) is taken as the computational domain Ω. As illustrated in Figure 5, the key nodes defining the boundaries of the reaches are alphabetically labeled A to H, and the y direction in each reach is identified. The key nodes are referred to as the upstream-ends (A, F, G, and H), the downstream-end (E), and the junctions (B, C, and D) serving as the confluence points in the channel network. Flow field in the domain is steady. Each reach is divided into 100 uniform elements, resulting in totally $N_e = 350$ elements with $N_n = 351$ nodes. The channel length L and the cross-sectional average velocity V for the reaches are specified according to Ramirez (2011) as shown in Table 2. The dispersivity D is set as

$$D = \alpha |V| + \varepsilon \tag{57}$$

where α and ε are positive constants. Here, α and ε are set as 0.1 and 1.0×10^{-6}, respectively. The decay coefficient R is considered two cases, which are of $R = 0$ (Test L1D-a) and $R = 0.005$ (Test L1D-b) over the domain. The ADE (12) is solved under the boundary conditions

$$M_1(y) = 0 \text{ at E} \tag{58}$$

and

$$D\frac{\partial M_1}{\partial y} = 0 \text{ at A, F, G, and H.} \tag{59}$$

Analytical MRT distributions are obtained by assuming global continuity of M_1 and the internal boundary conditions of the form (APPENDIX C)

$$\sum_{j=1}^{\nu_{\text{junc}}} \left[D\frac{\partial M_1}{\partial y} \right]_{j,\text{junction}} = 0 \tag{60}$$

at the junctions B, C, and D where ν_{junc} is the total number of reaches connected to the junction. The analytical MRT distributions do not have local extrema inside of the domain Ω, taking the minimum value 0 at the downstream-end E. Comparisons of the computed and the analytical MRT distributions for Tests L1D-a and L1D-b are shown in Figure 6. The computed MRT distributions

have no local extrema and there is an excellent agreement between the computed and analytical results, showing that the proposed PGFEM scheme correctly deals with the junctions.

Table 2 Specified values of L and V in each reach (Ramirez, 2011).

	A-B	B-C	C-D	D-E	F-B	G-C	H-D
L (m)	43.8	93.6	107.6	88.3	42.3	59.9	50.1
V (m/s)	0.78	1.04	1.11	1.05	0.91	0.86	0.83

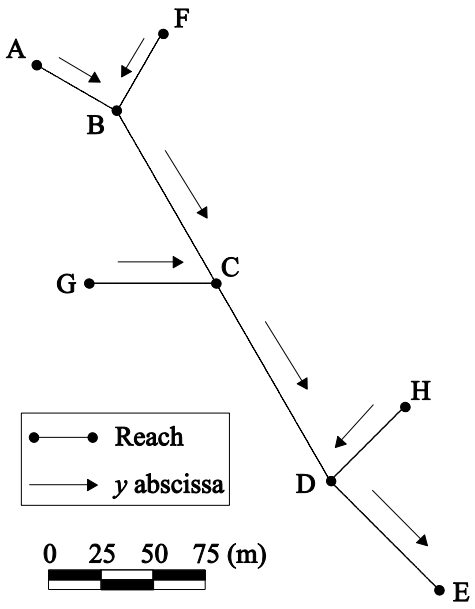

Figure 5 Plane view of the simply-connected open channel network with key nodes (Ramirez, 2011).

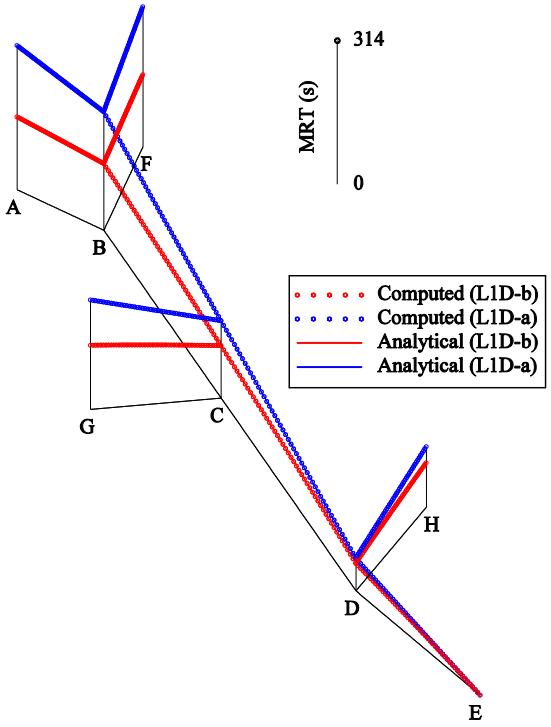

Figure 6 Comparisons of the computed and the analytical MRT distributions.

5. APPLICATION TO REAL LIFE PROBLEMS

5.1 Computational Domain

The verified PGFEM scheme is applied to numerical analysis of contaminant transport phenomena in an existing domain. A multiply-connected open channel network draining hydromorphic farmlands in the Guinea savanna agro-ecological zone of Ghana (Unami and Alam, 2012) is taken as the computational domain. Figure 7 illustrates a plane view of the channel network as the computational domain with finite element mesh and key nodes alphabetically labeled from A to P. Total numbers of elements and nodes in the domain are $N_e = 228$ and $N_n = 224$, respectively. The channel network consists of a main loop (A-B-C-D-E-F-A-G-H-I) running in the rice field, a downstream gully (K-L-M-N-O-J-P), and steep cliffs connecting the main loop and the gully (F-L, A-M, G-N, H-O, and I-J). The node D is the highest point in the domain, K and P are the boundaries, A, F, G, H, J, L, M, N, and O are the junctions. The node P is the downstream-end of the domain where a free-overflow natural weir is installed. The water input into the channel network is direct rainfall and lateral groundwater seepage from the farmlands (Unami et al., 2007). Water flows in the channel network exhibit highly complicated natures including both subcritical and supercritical flows due to the complex topography of the channel.

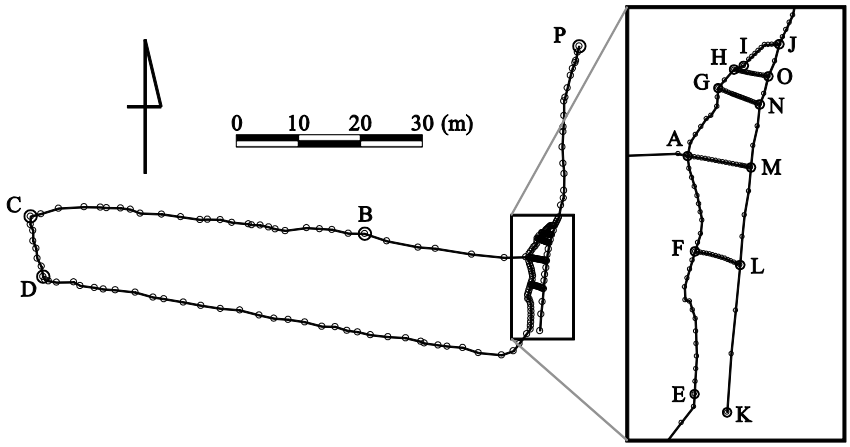

Figure 7 Plane view of the multiply-connected open channel network domain with computational mesh and key nodes.

5.2 Computational Conditions

The computed flow field in Unami and Alam (2012) is used for determining distributions of the known functions V and D in the domain. The cross-sectional velocity V is directly calculated from the flow field and the dispersivity D is estimated using the following stochastic theory based analytical formula (APPENDIX D)

$$D = \frac{\alpha |V|^{\beta-2} \Theta^{8/3}}{8 g^2 n^4}, \tag{61}$$

where α and β are positive parameters, Θ is the hydraulic radius, g is the gravitational acceleration, n is the Manning's roughness coefficient. Here, α and β are set as 5.00 and 2.25 in order to provide realistic distribution of D. The decay coefficient R is set as 0 (Case OC-1) or 0.0005 (Case OC-2) over the domain. The boundary nodes K and P are treated as the wall boundary Γ_{W} and the open boundary Γ_{O}, respectively. The statistical moments M_1 and M_2, and the escape probability E_{P} from the downstream-end P are computed using the PDE model with the PGFEM scheme. The total simulation period T is 30,000 (s), 10:10 a.m. on September 1st, 2009, is set as the time $s = 0$ and 6:30 p.m. on September 1st, 2009, is set as the terminal time $s = T$. The time increment Δs and the parameter θ are fixed to –0.01 (s) and 0.5, respectively. For computational purpose, the terminal conditions (13) and (18) are replaced with

$$M_k(T, y) = 0 \ \text{ in } \ \Omega \ \text{ for } \ k = 1, 2 \tag{62}$$

and

$$E_{\mathrm{P}}(T, y) = 1 \ \text{ in } \ \Omega. \tag{63}$$

5.3 Computational Results

Computational results of the spatially distributed statistics for Cases OC-1 and OC-2 are presented, focusing on the time series at the highest point D where the MRT M_1 mainly attains the maximum

values. Figure 8 and Figure 9 show time series of rainfall intensity, the MRT $M_{1,\mathrm{D}}$ at the node D and its deviations $M_{1,\mathrm{D}}-\sqrt{\Sigma_{\mathrm{D}}}$ and $M_{1,\mathrm{D}}+\sqrt{\Sigma_{\mathrm{D}}}$, and the escape probability $E_{\mathrm{P,D}}$ at the node D where $\sqrt{\Sigma}=\sqrt{M_2-\left(M_1\right)^2}$ represents the standard deviation of residence time. Non-negativity of M_1, M_2, and E_{P} were completely maintained in the entire simulation period. In Case OC-1, the escape probability E_{P} is 1 over the domain at all times implying that all the contaminant particles eventually flow out from the domain. In Case OC-2, increase of $M_{1,\mathrm{D}}$ and decrease of $E_{\mathrm{P,D}}$ occur simultaneously, and vice versa. This is considered to be reasonable since larger (smaller) residence time with $R>0$ results in more (less) contaminant killing and thus lower (higher) escape probability. Time evolution of $M_{1,\mathrm{D}}$ and $\sqrt{\Sigma_{\mathrm{D}}}$ are clearly inter-connected, and $\sqrt{\Sigma_{\mathrm{D}}}$ generally attains larger values in Case OC-1 than in Case OC-2. This is caused by the larger value of R in Case OC-2 which results in enhancing the variance of killing time as well as the second-order moment M_2. Although no experimental data to be compared is available, the computational results are consistent with intuitive expectations.

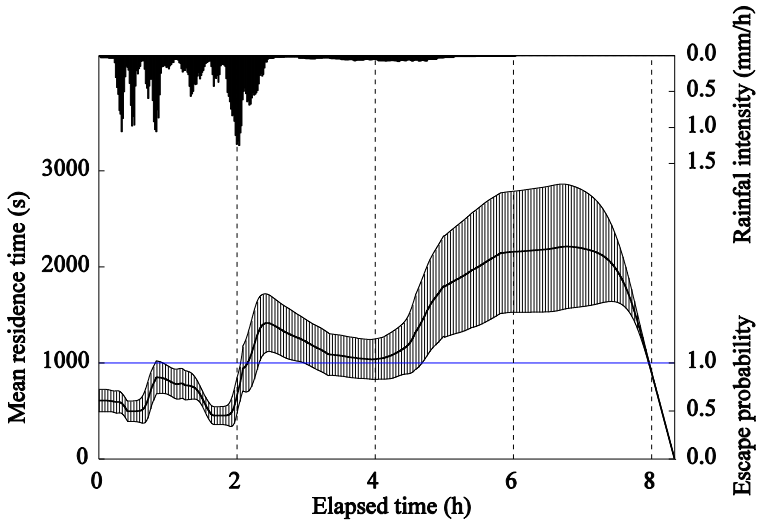

Figure 8 Rainfall intensity, the MRT $M_{1,\mathrm{D}}$ at the node D with its deviations $M_{1,\mathrm{D}}-\sqrt{\Sigma_{\mathrm{D}}}$ and $M_{1,\mathrm{D}}+\sqrt{\Sigma_{\mathrm{D}}}$, and the escape probability $E_{\mathrm{P,D}}$ at the node D for the Case OC-1.

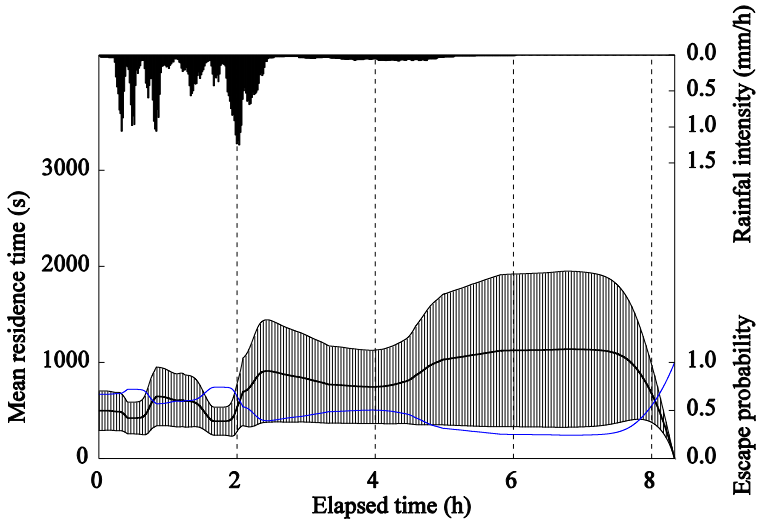

Figure 9 Rainfall intensity, the MRT $M_{1,\mathrm{D}}$ at the node D with its deviations $M_{1,\mathrm{D}} - \sqrt{\Sigma_{\mathrm{D}}}$ and $M_{1,\mathrm{D}} + \sqrt{\Sigma_{\mathrm{D}}}$, and the escape probability $E_{\mathrm{P,D}}$ at the node D for the Case OC-2.

6. CONCLUSIONS

The PDE model for spatio-temporal evolution of the spatially distributed statistics was proposed to efficiently analyze contaminant transport phenomena in locally one-dimensional open channel networks. The model is based on the KBE for contaminant particle transport and is not grounded on the gradient type laws. Each spatially distributed statistics was rigorously defined using the conditional PDF and then the linear time-backward ADEs comprising the model were derived.

A semi-implicit PGFEM scheme was introduced for accurate numerical resolution of the PDE model. In the scheme, a fitting technique is incorporated in order to produce oscillation-free numerical solutions with compact stencil. Then, junctions in the domains are consistently dealt with since the internal boundary conditions are implicitly included in spatial discretization of the scheme. Stability analysis based on the *M*-matrix theory showed that the scheme completely satisfies the elliptic discrete maximum principle as well as the parabolic discrete maximum principle with sufficiently fine time increment.

A series of test problems was examined to verify the PGFEM scheme. Computational results showed that the scheme produces excellently accurate numerical solutions for the steady test problems. However, computational results for the unsteady test problems indicated that time accuracy of the scheme should be improved. Possible options to improve time accuracy of the scheme are to use sufficiently fine computational mesh or to implement higher order temporal integration method such as the Padé approximation based method (Tian and Yu, 2010). Numerical analysis of contaminant transport phenomena in an existing multiply-connected open channel network was also carried out to assess applicability of the PDE model with the PGFEM scheme to problems in real life. Distributions of the spatially distributed statistics were successfully computed with the assumed dispersivity. Although no experimental data to be compared is available, the obtained results are considered to have reasonable accuracy.

It is concluded that the PDE model with the PGFEM scheme serves as an efficient and reliable tool for contaminant transport analysis in open channel networks. The theory and the method developed in this study are versatile, and thus they can be applied to quite a wide range of transport

phenomena in surface water flows. Future work will include sensitivity analysis of the PDE model, more detailed accuracy analysis of the PGFEM scheme, and application of them to important practical problems.

ACKNOWLEDGEMENTS

A part of this research is supported by the Japan Society for the Promotion of Science under grant 20255012 and the grant from the Japanese Society of Irrigation, Drainage and Rural Engineering.

REFERENCES

Chatwin, P.C. and Allen, X.N. (1985) "Mathematical Models of Dispersion in Rivers and Estuaries", Annual Reviews of Fluid Mechanics, Vol. 17, pp 119-149.

Øksendal, B. (2001) Stochastic Differential Equations, Springer-Verlag publishing company, Berlin.

Bodo, B.A., Thompson, M.E., Unny, T.E. (1987) "A Review on Stochastic Differential Equations for Applications in Hydrology", Stochastic Hydrology and Hydraulics, Vol. 1, pp 81-100.

Charles, W.M., Heemink, A.W., van de Berg, E. (2009) "Coloured Noise for Dispersion of Contaminants in Shallow Waters", Applied Mathematical Modelling, Vol. 33, pp 1158-1172.

Oh, J. and Tsai, W. (2010) "A Stochastic Jump Diffusion Particle-tracking Model (SJD-PTM) for Sediment Transport in Open Channel Flows", Water Resources Research, Vol. 46, W10508, 20 pp.

Too, J.R., Fan, L.T., Nassar, R. (1986) "A Stochastic Axial Dispersion Model for Tubular Flow Reactors", Chemical Engineering Science, Vol. 41, No.9, pp 2341-2346.

Man, C. and Tsai, C.W. (2007) "Stochastic Partial Differential Equation-Based Model for Suspended Sediment Transport in Surface Water Flows", Journal of Hydraulic Engineering, Vol. 133, No. 4, pp 422-430.

Yoshioka, H., Unami, K., Kawachi, T. (2012) "Stochastic Process Model for Solute Transport and the Associated Transport Equation", Applied Mathematical Modelling, Vol. 36, pp 1796-1805.

Yoshioka, H. (2012) "Parabolic Equation Models for Stochastic Transport Phenomena in Surface Water Flows", Master thesis, Water Resources Engineering Laboratory, Graduate School of Agriculture, Kyoto University, 2012.

Naeh, T., Klosek, M.M., Matkowsky, B.J., Schuss, Z. (1990) "A Direct Approach to the Exit Problem", SIAM Journal of Applied Mathematics, Vol. 50, No.2, pp 595-627.

Cai, G.Q., Qiu, X., Su, T.C., Lin, Y.K. (1996) "Markov Process Modeling of Groundwater Contamination Problems", Probabilistic Engineering Mechanics, Vol. 11, pp 243-250.

Brannan, J.R., Duan, J., Ervin, V.J. (1999) "Escape Probability, Mean Residence Time and Geophysical Fluid Particle Dynamics", Physica D, Vol. 133, pp 23-33.

Brannan, J.R., Duan, J., Ervin, V.J. (2001) "Escape Probability and Mean Residence Time in Random Flows with Unsteady Drift", Mathematical Problems in Engineering, Vol. 7, pp 55-65.

Szurley, J.R. and Duan, J. (2001) "The Effects of Changing Corioris Force Gradient Parameter on the Escape Probability and Mean Residence Time", Applied Mathematics and Computation, Vol. 118, pp 261-273.

Unami, K., Ishida, K., Kawachi, T., Maeda, S., Takeuchi, J. (2010) "A Stochastic Model for Behavior of Fish Ascending an Agricultural Drainage System", Paddy and Water Environment, Vol. 8, pp 105-111.

Yoshioka, H., Unami, K., Kawachi, T. (2011) "An Upwind Finite Element Scheme for Stochastic Contaminant Particle Dynamics in Locally One-dimensional Open Channel Networks", PAWEES 2011 International Student's Conference, 16 pp.

Lejay, A. (2003a) "Simulating a Diffusion on a Graph. Application to Reservoir Engineering", Monte Carlo Methods and Applications, Vol. 9, No.3, pp 241-256.

Lejay, A. (2003b) "Monte Carlo Methods for Fissured Porous Media: Gridless Approaches", IV IMACS Seminar on Monte Carlo Methods Vol. 10, No. 3-4, pp 385-292.

McGechan, M.B., Lewis, D.R., Vinten, A.J.A. (2008) "A River Water Pollution Model for Assessing of Best Management Practices for Livestock Farming", Biosystems Engineering, Vol. 99, pp 292-303.

Ngyuen, A.D. and Savenije, H.H.G. (2006) "Salt Intrusion in Multi-channel Estuaries: A Case Study in the Mekong Delta, Vietnam", Hydrology and Earth System Sciences, Vol.10, pp 743-754.

Grant, E.H.C., Lowe, W.H., Fagan, W.F. (2007) "Living in the Branches: Population Dynamics and Ecological Processes in Dendritic Networks", Ecology Letters, Vol. 10, pp 165-175.

Unami, K. (1998) "Optimization and Control of Water Conveyance/Storage Systems", Doctoral Thesis in Graduate School Agriculture, Kyoto University, pp 20-24.

NG-Stynes, M.J., O'Riordan, E., Stynes, M. (1988) "Numerical Methods for Time-dependent Convection-diffusion equations", Journal of Computational and Applied Mathematics, Vol. 21, pp 289-310.

de Falco, C. and O'Riordan, E. (2011) "A Parameter Robust Petrov-Galerkin Scheme for Advection-diffusion-reaction Equations", Numerical Algorithms, Vol. 56, pp 107-127.

Valkov, R.L. (2012) "Petov-Galerkin Analysis for a Degenerate Parabolic Equation in Zero-Coupon Bond Pricing", Large Scale Scientific Computing Lecture Notes in Computer Science, Vol. 7116, Springer-Verlag publishing company, Berlin, Heidelberg, pp 654-651.

Szymkiewicz, R. (2010) Numerical Modeling in Open Channel Hydraulics, Springer publishing company.

Abbott, M.B. (1979) Computational Hydraulics: Elements of Theory of Free Surface Flows, Pitman publishing company.

Von Below, J. (1988) "Classical Solvability of Linear Parabolic Equations on Networks", Journal of Differential Equations, Vol. 72, pp 316-337.

Freidlin, M. and Sheu, S. (2000) "Diffusion Processes on Graphs: Stochastic Differential Equations, Large Deviation Principle", Probability Theory and Related Fields, Vol. 116, pp 181-220.

Arnold, L. (1974) Stochastic Differential Equations: Theory and Applications, Wiley-Interscience publishing company.

Delhez, E.J.M., Heemink, A.W., Deleersnijder, E. (2004) "Residence Time in a Semi-enclosed Domain from the Solution of an Adjoint Problem", Estuarine, Coastal and Shelf Science, Vol.61, No. 4, pp 691-702.

Schuss, Z. (2010) Theory and Applications of Stochastic processes, Springer-Verlag publishing company, Newyork.

Benichou and Debsbois (2009) "Exit and Occupation Times for Brownian Motion on Graphs with General Drift and Diffusion Constant", Journal of Physics: Mathematical and Theoretical, Vol. 42, 015004, 24pp.

Gilberg, D. and Trundinger N.S. (1977) Elliptic partial differential equations of second order, Springer-Verlag publishing company, Berlin, Heidelberg.

Knabner, P. and Angermann, L. (2003) Numerical methods for elliptic and parabolic partial differential equations, Springer-Verlag publishing company.

Hundsdorfer, W. and Verwer, J.G. (2007) Numerical Solution of Time-dependent Advection-diffusion-reaction Equations, Springer-Verlag publishing company, Newyork.

Idelsohn, S., Nigro, N., Storti, M., Buscaglia, G. (1996) "A Petrov-Galerkin Formulation for Advection-reaction-diffusion Problems", Computer Methods in Applied Mechanics and Engineering, Vol. 136, pp 27-46.

Quarteroni, A. and Valli, A. (2008) Numerical Approximation of Partial Differential Equations, Springer-Verlag publishing company, Berlin, Heidelberg.

Mincsovics, M.E. (2010) "Discrete and Continuous Maximum Principles for Parabolic and Elliptic Operators", Journal of Computational and Applied Mechanics, Vol. 235, pp 470-477.

Farrel, P.A., Hegarty, A.F., Miller, J.J.H., O'Riordan, E., Shishkin, G.I. (2004) "Global Maximum Norm Parameter-uniform Numerical Method for a Singularly Perturbed Convection-dominated Problem with Discontinuous Convection Coefficient", Mathematical and Computational Modelling, Vol. 40, pp 1375-1392.

Guo, W. and Stynes, M. (1994a) "Finite Element Analysis of Exponentially Fitted Lumped Schemes for Time-dependent Convection-diffusion Problems", Numerische Mathematik, Vol. 66, pp 347-371.

Guo, W. and Stynes, M. (1994b) "Finite Element Analysis of an Exponentially Fitted Non-lumped Scheme for Advection-diffusion Equations", Applied Numerical Mathematics, Vol. 15, pp 375-393.

Ramirez, J.M. (2011) "Population Persistence under Advection-diffusion in River Networks", Journal of Mathematical Biology, 21 pp.

Unami, K. and Alam, A.H.M.B. (2012) "Concurrent Use of Finite Element and Finite Volume Methods for Shallow Water Flows in Locally 1-D Channel Networks", International journal of Numerical Method in Fluids, Vol. 69, No. 2, pp 255-272.

Unami, K., Kawachi, T., Kranjac-Berisavljevic, G., Abagale, F.K., Maeda, S., Takeuchi, J. (2007) "Case study: Hydraulic Modeling of Runoff Processes in Ghanian Inland Valleys". Journal of Hydraulic Engineering, Vol. 135, No. 7, pp 539-553.

Tian, Z.F. and Yu, P.X. (2011) "A Higher-order Exponential Scheme for Solving 1D Unsteady Convection-diffusion Equations", Journal of Computational and Applied Mathematics, Vol. 235, pp 2477-2491.

Funaki, N. (2005) Stochastic Differential Equations, Iwanami publishing company (in Japanese).

Yoshioka, H., Unami, K., Kawachi, T. (2011) "A Stochastic Process Model of Local Velocity for One-dimensional Open Channel Flows and Its Application to the Analysis of Advection-dispersion Problems", Proceedings of The Annual Conference on Applied Hydraulics, pp 30-33 (in Japanese).

APPENDICES

APPENDIX A

This APPENDIX gives the analytical expressions of the integrals $I_{i,j,0}$ and $I_{i,j,1}$ defined in (42). By (34) and (42), $I_{i,j,0}$ is calculated as

$$
\begin{aligned}
I_{i,j,0} &= \int_{\Omega_{\kappa(i,j)}} w_i \left(1 - \frac{y - y_i}{\sigma_{i,j} l_{\kappa(i,j)}}\right) \mathrm{d}y \\
&= \sigma_{i,j} l_{\kappa(i,j)} \int_0^1 \frac{\exp\left(\lambda_{i,j}^+ + \lambda_{i,j}^- z_{i,j}\right) - \exp\left(\lambda_{i,j}^- + \lambda_{i,j}^+ z_{i,j}\right)}{\exp\left(\lambda_{i,j}^+\right) - \exp\left(\lambda_{i,j}^-\right)} \left(1 - z_{i,j}\right) \mathrm{d}z_{i,j} \\
&= \frac{\sigma_{i,j} l_{\kappa(i,j)}}{\exp\left(\lambda_{i,j}^+\right) - \exp\left(\lambda_{i,j}^-\right)} \begin{bmatrix} \exp\left(\lambda_{i,j}^+\right) \int_0^1 \left(1 - z_{i,j}\right) \exp\left(\lambda_{i,j}^- z_{i,j}\right) \mathrm{d}z_{i,j} \\ -\exp\left(\lambda_{i,j}^-\right) \int_0^1 \left(1 - z_{i,j}\right) \exp\left(\lambda_{i,j}^+ z_{i,j}\right) \mathrm{d}z_{i,j} \end{bmatrix} \\
&= \frac{\sigma_{i,j} l_{\kappa(i,j)}}{\exp\left(\lambda_{i,j}^+\right) - \exp\left(\lambda_{i,j}^-\right)} \left[\exp\left(\lambda_{i,j}^+\right) F_1\left(\lambda_{i,j}^-\right) - \exp\left(\lambda_{i,j}^-\right) F_1\left(\lambda_{i,j}^+\right)\right]
\end{aligned}
\tag{64}
$$

where the change of variables from y to $z_{i,j}$ in (27) is applied in the second line of (64) and the function $F_1(\lambda)$ is defined as

$$
F_1(\lambda) = \int_0^1 (1 - z) \exp(\lambda z) \mathrm{d}z = \frac{\exp(\lambda) - \lambda - 1}{\lambda^2}. \tag{65}
$$

Similarly, $I_{i,j,1}$ is calculated as

$$
\begin{aligned}
I_{i,j,1} &= \int_{\Omega_{\kappa(i,j)}} w_i \left(\frac{y - y_i}{\sigma_{i,j} l_{\kappa(i,j)}}\right) \mathrm{d}y \\
&= \frac{\sigma_{i,j} l_{\kappa(i,j)}}{\exp\left(\lambda_{i,j}^+\right) - \exp\left(\lambda_{i,j}^-\right)} \left[\exp\left(\lambda_{i,j}^+\right) F_2\left(\lambda_{i,j}^-\right) - \exp\left(\lambda_{i,j}^-\right) F_2\left(\lambda_{i,j}^+\right)\right]
\end{aligned}
\tag{66}
$$

where

$$
F_2(\lambda) = \int_0^1 z \exp(\lambda z) \mathrm{d}z = \frac{(\lambda - 1)\exp(\lambda) - 1}{\lambda^2}. \tag{67}
$$

APPENDIX B

This APPENDIX proves that the matrix $-\mathrm{N}$ in (53) is an *M*-matrix. An *M*-matrix is a diagonally dominant matrix with positive diagonal entries and non-negative off-diagonal entries. In order to prove that $-\mathrm{N}$ is an *M*-matrix, it is sufficient to show that N is a diagonally dominant matrix with negative diagonal entries and positive off-diagonal entries. Firstly, the first term of the right hand side of (45) is rewritten as

$$
\begin{aligned}
\sum_{j=1}^{\nu(i)} \left[\left(w_i V - D_{i,j,0} \frac{\partial w_i}{\partial y}\right) u\right]_{\partial\Omega_{\kappa(i,j)}} &= \sum_{k=1}^{N_\mathrm{n}} N_{i,k} u_k \\
&= N_{i,l} u_i + \sum_{j=1}^{\nu(i)} N_{i,\mu(i,j)} u_{\mu(i,j)}
\end{aligned}
\tag{68}
$$

and each $N_{i,k}$ is given by

$$N_{i,k}=\begin{cases}-\sum_{j=1}^{\nu(i)}\sigma_{i,j}\left(V_{\kappa(i,j)}-D_{i,j,0}\left.\frac{\partial w_i}{\partial y}\right|_{y\to y_i}\right), & i=k\\ -\sigma_{i,j}D_{i,j,0}\left.\frac{\partial w_i}{\partial y}\right|_{y\to y_{\mu(i,j)}}, & k=\mu(i,j)\\ 0, \quad \text{Otherwise} & \end{cases} \tag{69}$$

where the limits $y\to y_i$ and $y\to y_{\mu(i,j)}$ are taken within the element $\Omega_{\kappa(i,j)}$. Comparing (27) and (69) shows that the off-diagonal entries of N are positive. Next, the diagonal entry $N_{i,i}$ is recast as

$$\begin{aligned}N_{i,i}&=-\sum_{j=1}^{\nu(i)}\sigma_{i,j}\left(V_{\kappa(i,j)}-D_{i,j,0}\left.\frac{\partial w_i}{\partial y}\right|_{y\to y_i}\right)\\ &=-\sum_{j=1}^{\nu(i)}\sigma_{i,j}\left(V_{\kappa(i,j)}\left(w_i\big|_{y\to y_i}-w_i\big|_{y\to y_{\mu(i,j)}}\right)+D_{i,j,0}\left(\left.\frac{\partial w_i}{\partial y}\right|_{y\to y_{\mu(i,j)}}-\left.\frac{\partial w_i}{\partial y}\right|_{y\to y_i}\right)-D_{i,j,0}\left.\frac{\partial w_i}{\partial y}\right|_{y\to y_{\mu(i,j)}}\right),\\ &=\sum_{j=1}^{\nu(i)}\left[\int_{\Omega_{\kappa(i,j)}}\left(-D_{i,j,0}\frac{\partial^2 w_i}{\partial^2 y}+V_{\kappa(i,j)}\frac{\partial w_i}{\partial y}\right)\mathrm{d}y-\sigma_{i,j}\left.\frac{\partial w_i}{\partial y}\right|_{y\to y_{\mu(i,j)}}\right]\end{aligned} \tag{70}$$

substituting (31) and (69) into (70) yields

$$\begin{aligned}N_{i,i}&=\sum_{j=1}^{\nu(i)}\left[\int_{\Omega_{\kappa(i,j)}}\left(-D_{i,j,0}\frac{\partial^2 w_i}{\partial^2 y}+V_{\kappa(i,j)}\frac{\partial w_i}{\partial y}\right)\mathrm{d}y-\sigma_{i,j}\left.\frac{\partial w_i}{\partial y}\right|_{y\to y_{\mu(i,j)}}\right]\\ &=\sum_{j=1}^{\nu(i)}\left[\int_{\Omega_{\kappa(i,j)}}\left(-R_{\kappa(i,j)}w_i\right)\mathrm{d}y-N_{i,\mu(i,j)}\right]\\ &=-\sum_{j=1}^{\nu(i)}\left[\int_{\Omega_{\kappa(i,j)}}R_{\kappa(i,j)}w_i\mathrm{d}y+N_{i,\mu(i,j)}\right]\end{aligned}. \tag{71}$$

Negativity of $N_{i,i}$ follows from the positivity of $N_{i,\mu(i,j)}$. Finally, diagonal dominance of N is confirmed by the inequality

$$\begin{aligned}\left|N_{i,i}\right|-\sum_{i\neq k}^{N_n}\left|N_{i,k}\right|&=\left|N_{i,i}\right|-\sum_{j=1}^{\nu(i)}\left|N_{i,\mu(i,j)}\right|\\ &=-N_{i,i}-\sum_{j=1}^{\nu(i)}N_{i,\mu(i,j)}\\ &=\sum_{j=1}^{\nu(i)}\left[\int_{\Omega_{\kappa(i,j)}}R_{\kappa(i,j)}w_i\mathrm{d}y+N_{i,\mu(i,j)}\right]-\sum_{j=1}^{\nu(i)}N_{i,\mu(i,j)}\\ &=\sum_{j=1}^{\nu(i)}\int_{\Omega_{\kappa(i,j)}}R_{\kappa(i,j)}w_i\mathrm{d}y\geq 0\end{aligned}, \tag{72}$$

showing that the matrix $-\mathrm{N}$ as well as $-\mathrm{N}^{(m)}$ are *M*-matrices.

APPENDIX C

This APPENDIX derives the internal boundary condition (60). Without loss of generality, the domain Ω is assumed to consist of all ν_{P} reaches conversing at a node P as shown in Figure 10. Each reach is given as a finite interval. The y abscissa in the jth reach starts from the node P and is denoted by y_j. The weight function w associated with the node P is then defined as

$$w_{\mathrm{P}} = \max\left(\frac{\varepsilon - y_j}{\varepsilon}, 0\right) \quad \text{in the } j\text{th reach} \tag{73}$$

where ε is a sufficiently small positive constant. The weak form (22) is rewritten as

$$\sum_{j=1}^{\nu_{\mathrm{P}}} \int_0^{\varepsilon} w\left(\frac{\partial u}{\partial s} - Ru - f\right) \mathrm{d}y_j + \sum_{j=1}^{\nu_{\mathrm{P}}} \left[wD \frac{\partial u}{\partial y_j} \right]_{+0}^{\varepsilon} - \sum_{j=1}^{\nu_{\mathrm{P}}} \int_0^{\varepsilon} \frac{\partial}{\partial y_j}\left(we^{\phi} D\right) e^{-\phi} \frac{\partial u}{\partial y_j} \mathrm{d}y_j = 0 \tag{74}$$

where

$$\phi = -\int_0^{y} \frac{V(s, y')}{D(s, y')} \mathrm{d}y' . \tag{75}$$

By taking the limit $\varepsilon \to +0$, the first term and the second term of (74) vanish. On the other hand, the limit of the third term is calculated as

$$\begin{aligned}
\lim_{\varepsilon \to +0} \sum_{j=1}^{\nu_{\mathrm{P}}} \int_0^{\varepsilon} \frac{\partial}{\partial y_j}\left(we^{\phi} D\right) e^{-\phi} \frac{\partial u}{\partial y_j} \mathrm{d}y_j &= \lim_{\varepsilon \to +0} \sum_{j=1}^{\nu_{\mathrm{P}}} \int_0^{\varepsilon} \left(w \frac{\partial}{\partial y_j}\left(De^{\phi}\right) + De^{\phi} \frac{\partial w}{\partial y_j} \right) e^{-\phi} \frac{\partial u}{\partial y_j} \mathrm{d}y_j \\
&= \lim_{\varepsilon \to +0} \sum_{j=1}^{\nu_{\mathrm{P}}} \int_0^{\varepsilon} \left(\frac{y_j - \varepsilon}{\varepsilon} \frac{\partial}{\partial y_j}\left(De^{\phi}\right) + \frac{1}{\varepsilon} De^{\phi} \right) e^{-\phi} \frac{\partial u}{\partial y_j} \mathrm{d}y_j \\
&= \lim_{\varepsilon \to +0} \sum_{j=1}^{\nu_{\mathrm{P}}} \int_0^{\varepsilon} \left(\frac{y_j - \varepsilon}{\varepsilon} \frac{\partial}{\partial y_j}\left(De^{\phi}\right) e^{-\phi} \frac{\partial u}{\partial y_j} + \frac{1}{\varepsilon} D \frac{\partial u}{\partial y_j} \right) \mathrm{d}y_j , \\
&= 0 + \lim_{\varepsilon \to +0} \sum_{j=1}^{\nu_{\mathrm{P}}} \int_0^{\varepsilon} \left(\frac{1}{\varepsilon} D \frac{\partial u}{\partial y_j} \right) \mathrm{d}y_j \\
&= \sum_{j=1}^{\nu_{\mathrm{P}}} \left(D \frac{\partial u}{\partial y_j} \right)_{y_j = +0}
\end{aligned} \tag{76}$$

yielding the internal boundary condition at the node P as

$$\sum_{j=1}^{\nu_{\mathrm{P}}} \left(D \frac{\partial u}{\partial y_j} \right)_{y_j = +0} = 0 . \tag{77}$$

Internal boundary conditions for more general cases are derived in a similar way.

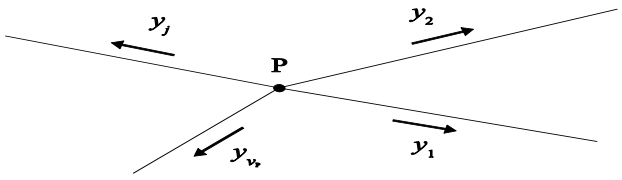

Figure 10 A schematic sketch of the reaches converging at a node.

APPENDIX D

This APPENDIX analytically derives the formula (61) of the dispersivity D. In the one-dimensional shallow water theory, the cross-sectional velocity v is damped by the Manning's friction law as

$$\frac{\mathrm{d}v}{\mathrm{d}t} = F - \frac{gn^2}{\Theta^{4/3}} v|v| \tag{78}$$

where F is the spatial differential terms. The cross-sectional velocity v is decomposed to the deterministic component V and the stochastic component W as

$$v = V + W . \tag{79}$$

Then, (78) is linearized around the deterministic component V and adding a stochastic fluctuation term to it obtains the governing equation of W as

$$\mathrm{d}W = -\psi W \mathrm{d}t + \sigma \mathrm{d}B_{t,x} \tag{80}$$

where $\psi = \dfrac{2gn^2|V|}{\Theta^{4/3}}$ is the attenuation characteristic of W, σ is a positive parameter, and $B_{t,x}$ is the space-time white noise (Funaki, 2005). The differential equation (80) is regarded as an infinite SDE. In the above framework, passive particle displacement X_t in the flow is described as

$$\frac{\mathrm{d}X_t}{\mathrm{d}t} = v = V + W . \tag{81}$$

In an infinite uniform flow, the parameters ψ and σ are considered to be constant and straightforward calculation shows that the variance $\mathrm{Var}\left[X_t\right]$ for a large time t is given by

$$\mathrm{Var}\left[X_t\right] = \frac{\sigma^2}{\psi^2} t \tag{82}$$

where X_0 is taken as 0 without loss of generality. On the other hand, the variance $\mathrm{Var}\left[X_t\right]$ at the time t is given by

$$\mathrm{Var}\left[X_t\right] = 2Dt . \tag{83}$$

Considering the statistical consistency between the two expressions (82) and (83), the dispersivity D is determined as

$$D = \frac{\sigma^2}{2\psi^2} = \frac{\sigma^2 \Theta^{8/3}}{8g^2 n^4 |V|^2} . \tag{84}$$

The same result has been obtained in Yioshioka et al. (2010). Further, assuming the velocity dependence of σ as

$$\sigma^2 = \alpha |V|^{\beta} \tag{85}$$

leads to (61).